Effects of Lewis Number on Temperatures of Spherical Diffusion Flames

K.J. Santa[*]
University of Hawaii, Honolulu, HI 96822

Z. Sun[†]
Washington University, St. Louis, MO 63130

B.H. Chao[‡]
University of Hawaii, Honolulu, HI 96822

P.B. Sunderland[§]
University of Maryland, College Park, MD 20742

R.L. Axelbaum[**]
Washington University, St. Louis, MO 63130

D.L. Urban[††] and D.P. Stocker[‡‡]
NASA Glenn Research Center, Cleveland, OH 44135

Spherical diffusion flames supported on a porous sphere were studied numerically and experimentally. Experiments were performed in 2.2 s and 5.2 s microgravity facilities. Numerical results were obtained from a Chemkin-based program. The program simulates flow from a porous sphere into a quiescent environment, yields both steady-state and transient results, and accounts for optically thick gas-phase radiation. The low flow velocities and long residence times in these diffusion flames lead to enhanced radiative and diffusive effects. Despite similar adiabatic flame temperatures, the measured and predicted temperatures varied by as much as 700 K. The temperature reduction correlates with flame size but characteristic flow times and, importantly, Lewis number also influence temperature. The numerical results show that the ambient gas Lewis number would have a strong effect on flame temperature if the flames were steady and nonradiating. For example, a 10% decrease in Lewis number would increase the steady-state flame temperature by 200 K. However, for these transient, radiating flames the effect of Lewis number is small. Transient predictions of flame sizes are larger than those observed in microgravity experiments. Close agreement could not be obtained without either increasing the model's thermal and mass diffusion properties by 30% or reducing mass flow rate by 25%.

I.   Introduction

Spherical diffusion flames are valuable tools for understanding nonpremixed combustion.[1–5] These flames are one-dimensional and are straightforward to model. The flames can be generated in microgravity using droplets or by issuing a gaseous or liquid reactant from a porous sphere. Unique features of the flame supported on a porous sphere include the ability to select the direction of convection from fuel to oxidizer (normal flame) or from oxidizer to fuel

---

[*] Research Assistant, Department of Mechanical Engineering, 2540 Dole St., #302.
[†] Research Assistant, Department of Mechanical and Aerospace Engineering, 208 Jolley Hall.
[‡] Associate Professor, Department of Mechanical Engineering, 2540 Dole St., #302.
[§] Assistant Professor, Department of Fire Protection Engineering, 3104 J.M. Patterson Bdg., AIAA Senior Member.
[**] Associate Professor, Department of Mechanical and Aerospace Engineering, 208 Jolley Hall.
[**]Chief, Combustion and Reacting Systems Branch, M.S. 77-5, AIAA Senior Member.
[††]Aerospace Engineer, Combustion and Reacting Systems Branch, M.S. 77-5.

(inverse flame) for given fuel and oxidizer concentrations (i.e., for a given stoichiometric mixture fraction, Z_{st}). The flames can have extremely low scalar dissipation rates, approaching those of purely diffusion (zero convection) flames.

Spherical diffusion flames have been employed to study the effects of Z_{st} on soot production[4] and sooting limits.[5] These results have shown, as have earlier works,[2] that the flames may not reach steady state during 2.2 s or even 5.2 s of microgravity. These flames generally have small scalar dissipation rates, which result in long times to reach steady state. Furthermore, small scalar dissipation rates result in large radiative losses from the gaseous products, which can significantly reduce flame temperatures compared to normal-gravity flames. To better understand the factors influencing transient spherical flames, and thus allow a clearer interpretation of past and future data, a systematic numerical study was undertaken to consider the influence of flow direction, stoichiometric mixture fraction, radiative heat loss and Lewis number (Le) on flame temperatures and sizes of spherical diffusion flames. In addition, measurements of the flame temperature and location were made in NASA's 2.2 s and 5.2 s drop facilities to assess the accuracy of the numerical results.

Flame structure can be influenced by the direction of convection across the flame (convection direction) and stoichiometric mixture fraction. The convection direction (either into the oxidizer or the fuel) is controlled by the selection of burner and ambient gases, while the stoichiometric mixture fraction is controlled by varying the amount of inert (e.g., nitrogen) in the fuel and/or oxidizer. Four ethylene flames have been studied, namely, those considered in our earlier work,[4] and they are described in Table 1. The four flames have the same adiabatic flame temperature, 2370 K, which is that of neat ethylene burning in air when the reactants are supplied at 300 K. They also have the same ethylene consumption rate, 1.51 mg/s. Sunderland et al.[4] includes a schematic diagram and sample images of these flames. Table 1 includes characteristic residence times, t_{res}, defined as the estimated mass of gas between the flame and the burner divided by the burner mass flow rate.[5]

In a spherical diffusion flame, only the Lewis number of the ambient gas (not that of the burner gas) has a significant effect on the flame.[6–8] For spherical flames burning in air this Le is near unity, but for inverse flames it depends on fuel properties and can deviate from unity. Since in this study the ambient gas composition is varied, we are able to study the influence of Le on these flames. The effect of Le could be significant in low-strained flames because diffusion distances will be greater and thus effects of unequal diffusion rates will be more pronounced. Law and Chung[6] found that for a one-dimensional chamber flame and a stagnation-point flame, blowing reduces the effects of Le when it follows the direction of diffusion and increases the effects when it opposes diffusion. The analytical theory showed that for a non-radiating one-dimensional chamber flame, a 10% reduction or increase in the Le from unity of the reactant supplied against the flow results in a 9% increase or 5% decrease in flame temperature. This is a much more significant effect than that observed in strained systems so one of the goals of this study is to determine if this effect can be realized in microgravity spherical flames.

Table 1. Test conditions for ethylene flames (a) – (d).

Flame	Burner Gas	Ambient Gas	$X_{C_2H_4}$	X_{O_2}	$Y_{C_2H_4}$	Y_{O_2}	Z_{st}	m_b, mg/s	t_{res}, s
(a)	C_2H_4	O_2 / N_2	1	0.21	1	0.233	0.064	1.51	2.19
(b)	C_2H_4 / N_2	O_2	0.0814	1	0.0815	1	0.78	18.6	0.046
(c)	O_2 / N_2	C_2H_4	1	0.21	1	0.233	0.064	22.2	0.091
(d)	O_2	C_2H_4 / N_2	0.0814	1	0.0815	1	0.78	5.18	0.893

II. Numerical

In the model a gaseous reactant is injected from the porous spherical burner at temperature T_b into an infinite quiescent environment of the other reactant at temperature T_∞. The burner is assumed to be perfectly symmetric so that the flow field and flame are spherically symmetric in microgravity. The numerical code is a modification of the PREMIX[9] code, adapted to a diffusion flame in a spherical geometry and allowing for optically thick radiative heat losses. For this problem, the equations describing the conservation of mass, energy and gas species are:

$$\frac{\partial \rho}{\partial t} + \frac{1}{r^2}\frac{\partial(r^2 \rho u)}{\partial r} = 0 \ , \tag{1}$$

$$\rho c_p \frac{\partial T}{\partial t} = \frac{1}{r^2} \frac{\partial}{\partial r}\left(r^2 \lambda \frac{\partial T}{\partial r}\right) - \rho u c_p \frac{\partial T}{\partial r} - \sum_{k=1}^{K}\left(\rho c_{pk} Y_k V_k \frac{\partial T}{\partial r} + h_k \omega_k Y_k\right) - Ra \quad , \tag{2}$$

$$\rho \frac{\partial Y_k}{\partial t} = -\frac{1}{r^2} \frac{\partial}{\partial r}\left(r^2 \rho Y_k V_k\right) - \rho u \frac{\partial Y_k}{\partial r} + W_k \omega_k Y_k \quad , \quad k = 1, 2, \ldots, K \quad , \tag{3}$$

where T is the temperature, Y_k is the mass fraction of species k, W_k is the molecular weight of species k, t is time, r is the radial spatial coordinate, u is the radial flow velocity, ρ is the gas density, c_p is the averaged specific heat at constant pressure, λ is the heat conductivity, h_k is the specific enthalpy of species k, $c_{p,k}$ is the specific heat of species k, V_k is the diffusion velocity of species k, ω_k is the production rate of species k, K is the number of species, and Ra is the rate of radiative heat loss. The equations were solved subject to the following boundary conditions

$$r = r_b \ : \ T = T_b \ ; \ Y_k(u + V_k) = u\, Y_{k,b} \ , \ k = 1, 2, \ldots, K \quad , \tag{4}$$

$$r \to \infty \ : \ T \to T_\infty \ ; \ Y_k \to Y_{k,\infty} \ , \ k = 1, 2, \ldots, K \quad , \tag{5}$$

where the subscripts 0, b and ∞ refer to conditions at the center of the burner, the burner surface and the ambient, respectively. Because thermocouple measurements in the 5.2 s drop facility showed no significant increase in burner surface temperature during the drop, T_b was taken to be constant. In addition, the results indicate that after 5 s the thermal field had only reached a radius of 9 cm from the center of the burner and the computations predicted no significant change in reactant compositions at a radius of 100 cm. Thus, while the computations assumed a finite domain ($r_{wall} = 100$ cm), it was effectively infinite and the results were not affected by this assumption. Both T_b and T_∞ were taken to be 300 K in this study.

Radiation was considered to be optically thick and caused only by the participation of CO_2, H_2O and CO. The radiative properties of these gases were formulated by a statistical narrow-band model with a spectral bandwidth of 25 cm^{-1}. The emissivities were extracted from the line-by-line values given by the HITRAN database.[10] To account for the angular variation of the radiation intensity, the discrete ordinates method was employed, with a discrete representation that included 20 different directions. The rate of radiative heat transfer was then evaluated by integrating over all directions using Gaussian quadrature. A more detailed description of the radiation model can be found in Carlson and Lathrop.[11]

Conventional finite difference techniques with non-uniform mesh spacing were adopted for the discretization of the differential equations. The transient terms were expressed by a forward difference formula, the diffusive terms by a central difference formula, and, for better convergence, the convective terms by an upwind difference formula. The discretized equations were solved by Sandia's Twopnt package,[12] which uses Newton's method to solve transient and steady-state boundary value problems. The chemical reaction rates, the thermodynamic properties, and the transport properties were evaluated by Chemkin and Transport software.[13,14] The kinetics data were provided by GRI-Mech 3.0, which contains 53 species and 325 reactions.[15] The number of grids was varied until the solution did not change with further addition of grids. The time step was adjusted until the solution converged.

Following the approach adopted in Tse et al.,[2] the initial (ignition) conditions for the transient cases were prescribed as the steady-state solutions of flames without radiation and with the same outer boundary values, but with the outer boundary brought to 1.2 cm from the burner exit. The temperature boundary condition at the burner exit was adiabatic. These conditions lead to a thin high-temperature ignition source near the burner surface, which is consistent with the conditions that would exist when a diffusion flame is first established after ignition (i.e., the gradients are steep and radiative losses are negligible).

III.   Experimental

The experiments were conducted in microgravity in the NASA Glenn Research Center 2.2 s and 5.2 s drop facilities. The experimental apparatus is described in detail in Sunderland et al.[4,5] The burner was a 6.4 mm diameter porous stainless-steel sphere. All tests were conducted in a pressure vessel of 26 liters initially at 0.98 bar (with an estimated uncertainty of $\pm$ 0.005 bar) and room temperature.

Each test involved three gases: a hydrocarbon fuel (typically ethylene), nitrogen, and oxygen. Purity of the fuels was 99.9% while that of nitrogen and oxygen was 99.999%. The test conditions are summarized in Tables 1 and 2.

For each test either fuel or oxygen was diluted with nitrogen. The various gas mixtures were prepared either gravimetrically or by partial-pressure mixing and had an estimated composition uncertainty of ±0.001 mole fraction. Both normal and inverse flames were considered, where the pressure vessel was initially filled with, respectively, oxidizer and fuel.

Table 2. Measured and modeled relative peak temperatures 1.9 s after ignition for inverse flames of three hydrocarbon fuels[a]

Burner Gas	Ambient Gas	Le_F[b] (300 K)	X_F	Y_F	Z_{st}	m_b mg/s	$T_{max} - T_{max,C_2H_4}$, K measured	modeled
O_2	CH_4 / N_2	0.92	0.14	0.0853	0.75	5.85	322[c]	152
O_2	C_2H_4 / N_2	1.37	0.0814	0.0815	0.78	5.18	0	0
O_2	C_3H_8 / N_2	1.98	0.058	0.0884	0.76	4.49	−275	−117

[a] Each of these flames has an adiabatic flame temperature of 2370 K. Note that the second flame here is ethylene Flame (d).
[b] The Le_F was estimated from Chemkin[13] where the thermal diffusivity is that of nitrogen and the mass diffusivity is that of the fuel into the fuel mixture.
[c] Lower bound owing to incipient saturation in the thin-film pyrometer.

Burner gas flow rates were measured under steady state, cold flow conditions in normal gravity about 30 minutes (for 2.2 s tests) or 90 minutes (for 5.2 s tests) before drop initiation. These flow rates were measured with a calibrated mass flow meter and were adjusted with a needle valve. Uncertainties in the burner flow rates are estimated at ±10%. At 2 s before drop initiation the two solenoid valves were opened to commence flow to the burner. The ignitor was energized in microgravity immediately after drop initiation and ignited the flames within 30 ms.

The flames were imaged using two cameras. For tests that did not involve thin-filament pyrometry (TFP) a color charge-coupled device (CCD) video camera was used. This camera had 640 × 480 pixels, 8 bits per color plane, a framing rate of 30 Hz, and a 16 mm manual-iris lens at f/1.4. Spatial resolution was 150 μm. The camera yielded flame appearance and average radius from ignition until drop termination. Except for Flame (c), flame radii were measured using the contours of peak blue emission in the video records. For Flame (c) only yellow (not blue) emissions were visible. Thus the radii for Flame (c) were measured using the inside of the contours of brightest yellow emissions. Flame diameters were determined by averaging the longest chord through each flame and its perpendicular chord; radii were then obtained by dividing the results by two.

For tests involving thin-filament pyrometry (in the 2.2 s drop tower) the video camera was replaced with a Nikon D100 consumer-grade color digital still camera. This camera has a CCD with 3008 × 2000 pixels (6 megapixels) and 12 bits per color plane. The lens that was used has a focal length of 60 mm and was set at f/8. Exposure time was 33 ms, ISO was 200, white balance was direct sunlight, and all automatic gain and focusing were disabled. Spatial resolution was 27 μm. Images from this camera were used to determine approximate peak temperatures and flame radii.

The TFP method used here was based on past work.[16–18] Three silicon carbide fibers, with diameters of 13.9 μm, were strung across the flames in the camera focal plane. Before each test they were heated to glowing in lean regions of a diffusion flame to remove any deposited soot. A solenoid triggered the shutter release, whereby the camera recorded four images at times of 0.1, 0.7, 1.3, and 1.9 s after drop initiation. The filament images were smoothed using 5 × 5 pixel binning. The brightest pixel greyscale was then recorded along each of the six fiber-flame crossings and these were averaged. These average grayscales were converted to relative fiber temperatures using the previous calibration for a similar TFP system of 0.215 K/greyscale.[18] These fiber temperatures were corrected for radiative loss.[18] An absolute temperature reference was obtained by a thermocouple measurement of the peak temperature for Flame (d) at 1.9 s.[4] The TFP temperatures were repeatable but have high estimated uncertainties of ±150 K owing to calibration uncertainties, slight soot deposition on the fibers, and incipient saturation in the red color plane for the methane test.

IV.   Results and Discussion

A. Numerical and Experimental

Computations were performed for ethylene Flames (a) − (d), defined in Table 1. The flame radius from the model was assumed to be the radius of the peak temperature. All flames initially grew with time, but Flames (b) and (c) approached steady state more rapidly than Flames (a) and (d) did because of their high flow velocities and low residence times (see Table 1). The initial growth can be understood from the fact that diffusion flames stabilize where the fluxes of oxidizer and fuel are in stoichiometric proportions. For the present transient flames, the consumption of the ambient reactant over time reduces the gradient and thus the flux to the flame. In response, the flames expand to reduce the burner reactant flux at the flame. The rate of variation of flame radii with time predicted by the model matches the experiments for Flame (b) after about 0.5 s and for Flames (a) and (d) after about 1 s. The initial difference in slopes is likely due to differences in initial (ignition) conditions between the model and experiments. The measured luminous radii of Flame (c) match the predicted flame radii. However the measured radii are only estimates because they were based on yellow emissions.

While the trends for Flames (a), (b), and (d) predicted by the model closely resemble those of the experiments, the model predicts larger flames. A similar discrepancy was observed in a previous study[2] and was accounted for by noting that the peak temperature occurs on the oxidizer side of the visible flame. Although this explanation would improve the agreement for Flames (a) and (b), it would reduce the agreement for Flames (c) and (d). The source of the discrepancy remains unclear, but it could arise from thermal and mass diffusion properties that are too low in the model or from experimental flow rates that are lower than reported, or a combination of both. Transport properties are based on the Lennard-Jones potential model,[19] which can underpredict transport properties of light species by up to 25%.[20,21]

To evaluate the effect of assumed transport properties, the thermal and mass diffusion properties in the model were varied. Figure 1 shows the results when transport properties were increased 30% above the values predicted by the Transport code[14] for Flames (a), (b), and (d). Flame (c) was not included in Fig. 1 owing to uncertainties in flame radius resulting from soot obscuration. Because both transport properties were increased, the Lewis number and the adiabatic flame temperature were unchanged. The agreement between model and experiment in Fig. 1 is good following this change. A similar improvement is observed following a reduction of 25% in the model's mass flow rate, but this exceeds the 10% estimated uncertainty in the experimental flow rate. Because the source of discrepancy between experiment and theory is unknown, the unmodified transport properties are used in the remainder of this work.

Predictions of transient peak flame temperatures for the four ethylene-fueled flames are shown in Fig. 2. Due to gaseous radiative heat loss the peak temperatures are predicted to decrease with time except near ignition. Although
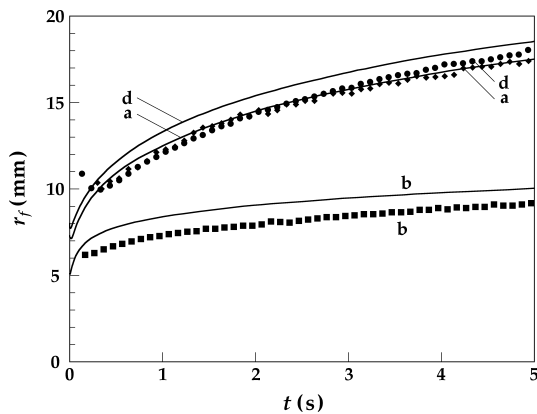
Figure 1. Predicted and measured flame radii for three ethylene flames, (a), (b), and (d), where the transport properties have been increased by 30%. The curves are numerical results while the synbols represent experiments in the 5.2 s drop facility. The modeled radii correspond to peak temperatures. The measurements were derived from video records.
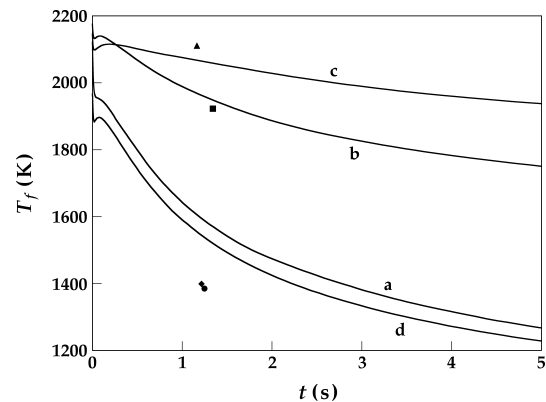
Figure 2. Evolution of peak flame temperature with time for ethylene Flames (a) − (d). The curves represent transient numerical results while the symbols represent thermocouple measurements in the 2.2 s drop tower, with legend as given in Fig. 1.

these four flames have the same adiabatic flame temperature (2370 K), the temperatures of Flames (a) and (d) are predicted to be markedly lower than those of Flames (c) and (b). As shown in Fig. 1, Flames (a) and (d) have roughly double the radii of the other flames. The larger flames have greater radiative losses, resulting in peak temperatures up to 700 K cooler than the other flames. In fact, even though these flames are quite different structurally, one being a low Z_{st} normal flame and the other a high Z_{st} inverse flame, they both have similar temperatures, indicating the dominant effect of flame size on radiative heat loss. However, flame size is not the sole factor affecting flame temperature. Comparison of flame temperatures of Flames (a) and (b) at a flame radius of 10 mm reveals a 115 K difference in flame temperature for the same flame radius. The higher temperature of Flame (b) is likely due to its shorter residence time (see Table 1) as a result of its higher flow rate.

Also shown in Fig. 2 are peak temperatures for these four flames as measured with thermocouples in the 2.2 s drop tower. Each symbol indicates an average temperature (previously reported in Sunderland et al.[4]) and an average measurement time (not previously reported) from repeat tests. These temperatures are radiation-corrected with estimated uncertainties of ±50 K.[4] The agreement between modeled and measured temperatures is within experimental uncertainties for Flames (b) and (c). The numerical predictions in the other two flames significantly over-predict the measured temperatures and this probably arises from different ignition conditions in the model and the experiment. For example, in the experiments there is about 2 s of reactant flow through the porous sphere before ignition. This results in a premixed flame that rapidly transitions to a diffusion flame but leaves products behind that enhance radiation and reduce flame temperature, which is consistent with the lower experimental temperature for Flames (a) and (d). Such differences are not evident for Flames (b) and (c) because the effects of ignition are convected outward more rapidly in those flames. These flames have a larger mass flow rate and a smaller flame radius, leading to much shorter characteristic residence times (see Table 1).

To understand the basic structural differences in the four flames without the complexity of transient effects and radiative heat loss, *steady-state* calculations without radiation were performed using the same code, and the results are plotted in Fig. 3. Because there is no heat loss to the burner in this simulation, and all four flames have the same equilibrium adiabatic flame temperature (2370 K), these four flames might be expected to have peak temperatures close to 2370 K. This is the case for Flames (a) – (c), but Flame (d) is about 200 K cooler.

Two factors may cause the reduced peak temperature of Flame (d) in this steady simulation. One is that Flame (d), unlike Flame (b), has fuel in the ambient, which could lead to a loss of intermediate species by diffusion into the ambient. Simulations of the losses of CO, H_2 and C_2H_2 to the ambient show that the 200 K reduction in flame temperature for steady Flame (d) cannot be due to the loss of intermediates.

A more plausible explanation for the reduced peak temperature of steady Flame (d) is that the Lewis number of the ambient reactant for this flame is higher than that of the others. *Le* is defined here as the mixture thermal diffusivity divided by the mass diffusivity of the reactant in the mixture. It is known that for spherical burner-supported and droplet flames the dominant *Le* affecting flame temperature is that on the ambient side of the flame.[7,8] While a reduction in temperature can occur when the ambient *Le* exceeds unity, a 200 K reduction might be considered large for Flame (d).

To observe the effects of non-unity Lewis number of the ambient reactant, computations were performed for Flame (d) in steady state using the same code, assuming ambient Le_F equal to, greater than and less than unity, and employing a simplified one-step reaction in the reaction-sheet limit. That is, the reaction rate was set to be sufficiently fast that further increases in reaction rate would not change the solution. The diffusivities for all species were made the same. Computations for Le_F of 0.9, 1.0, and 1.1 were performed and the results are shown in Fig. 4. With a 10% increase/decrease in Le_F, the flame temperature decreases/increases by about 200 K, in qualitative agreement with Law and Chung.[6] These results suggest that the difference in ambient *Le* between steady Flame (d) and the other flames accounts for the 200 K decrease observed in Fig. 3. Such Lewis number effect was not observed for the transient flames shown in Figs. 1 and 2 because of the growth of the flame. The outward expansion of the flame towards the ambient suppresses the significance of inward diffusion (against convection) required for the ambient reactant to reach the flame.

To verify that the Le_F of Flame (d) is higher than those of Flames (a) – (c), the variation of *Le* of the ambient reactant for these four flames is shown in Fig. 5. These results were obtained from the steady-state computations using the code described in Section 2 but without radiation, as in Fig. 3. A distance of 10 cm from the flame sheet was chosen as the domain of interest because diffusion of the ambient reactant is most important in this preheat region ahead of the flame. In the region of 4-10 cm from the flame there are two groupings: Flames (a) – (c) have nearly unity Lewis number and Flame (d) has a Lewis number of about 1.2. Closer to the flame, Flame (c) shows an increase in *Le* but because the fuel is in the ambient, the primary fuel already is decomposed here and thus the relevant *Le* is no longer that of the fuel, but rather some function of the *Le* of the intermediates. The
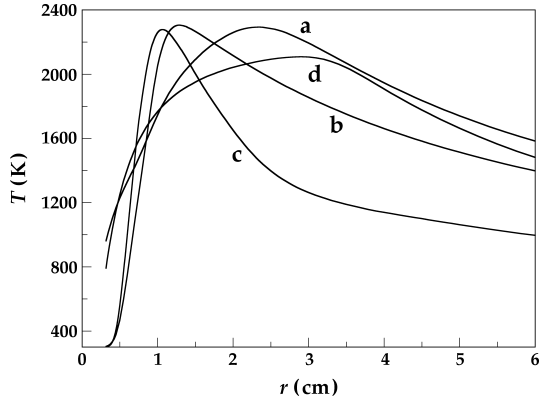
Figure 3. Steady-state solutions of the temperature distributions for ethylene Flames (a) – (d) without radiative heat loss.
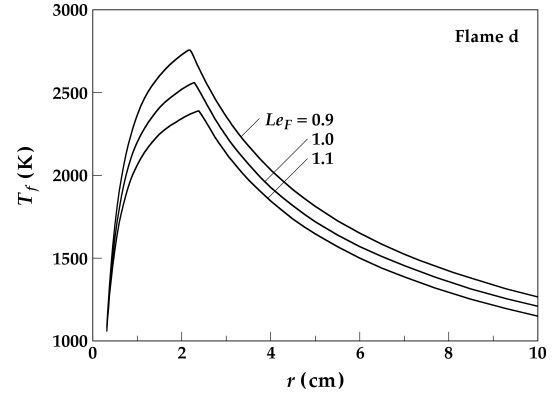

Figure 4. Steady-state solution of temperature profiles without radiative heat loss for ethylene Flame (d) with Lewis numbers of 0.9, 1.0, and 1.1. A one-step, reaction sheet limit was used in the simulation.

intermediates are smaller molecules, which have a greater diffusivity and thus a smaller Le. Thus, the primary finding from Fig. 5 is that in the diffusion zone approaching the flame, the Le of Flame (d) is approximately 20% greater than that of the other flames.

B. Analytical

An analysis that employs the Burke-Schumann reaction sheet limit was performed for steady inverse flames to better understand the effect of Lewis number. The analysis assumes constant transport properties, but allows different Lewis numbers on the fuel and oxidizer side of the flame. The solution yields the flame temperature, given by

$$T_f = \left(T_0 + \frac{v_F W_F}{v_O W_O}\frac{q_F}{c_p}Y_{O,0}\right) - \left(T_0 + \frac{v_F W_F}{v_O W_O}\frac{q_F}{c_p}Y_{O,0} - T_\infty\right)\left(\frac{v_F W_F Y_{O,0}}{v_F W_F Y_{O,0} + v_O W_O Y_{F\infty}}\right)^{1/Le_F}, \qquad (6)$$

where v_k is the stoichiometric coefficient of species k, q_F is the heat of combustion per unit mass of the fuel, T_0 is the supplied gas temperature at the center of the burner, and the subscripts F and O denote fuel and oxidizer. In Eq. (6), Le_F is the Lewis number of the fuel/nitrogen mixture, which for Flame (d) is the ambient reactant. As expected, the solution of Eq. (6) indicates that flame temperature depends only on the ambient-side Lewis number. In addition, flame temperature increases/decreases when the ambient Le_F is below/above unity. This analytical finding is consistent with the present numerical results and with earlier studies.[7,8]

The flame temperatures and the relative differences of flame temperature from the unity Lewis number flame for selected hydrocarbon flames, calculated using Eq. (6) for steady Flame (d), are plotted versus Le_F in Fig. 6. A variation in ambient Le can be affected by changing the ambient diluent (as in Fig. 4) and/or the fuel. For example, if N_2 were replaced with He here, an increase in Le would result, whereas with CO_2 a decrease would occur. The flame temperatures of the unity Le_F flames are calculated using the Chemical Equilibrium with Applications (CEA) code.[22] The value of (q_F/c_p) for each fuel is adjusted such that the flame temperatures obtained from Eq. (6) agree with those obtained from CEA. Figure 6 shows that all fuels have the same qualitative behavior in that flame temperature decreases with increasing Le. When the flame temperature is normalized relative to the value at unity Le, i.e., $T_f/T_f(Le_F=1)$, the data collapse to a single curve, as shown in Fig. 6, indicating that the relative change of flame temperature is independent of fuel type. Consistent with Fig. 4, in steady flames when Le_F is near unity a 10% increase in Le_F results in about a 200 K decrease in flame temperature, or about an 8% change. This effect increases with decreasing Lewis number, as previously reported.[6]
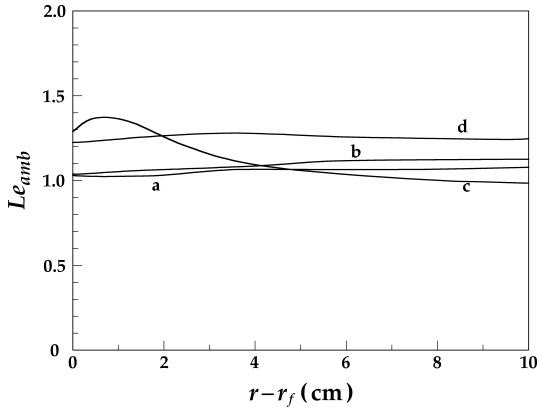
Figure 5. Variation of the Lewis number of the ambient reactant, Le_{amb}, versus the distance from the flame sheet for four ethylene flames. Results shown are for steady-state flames without radiative heat loss.
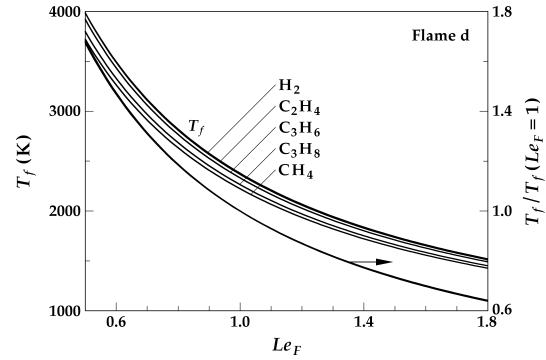

Figure 6. Flame temperature calculated using Eq. (6) versus Lewis number for Flame (d) for selected fuels. The lowest curve represents, for all fuels, the relative change of flame temperature from the unity Lewis number flame.

C. Results for other fuels

Figure 3, which does not include gaseous radiation, clearly shows the reduction in temperature for Flame (d), attributed to Le effects. Nonetheless, this finding is not readily apparent in the experimental and numerical results in Fig. 2, owing to the different radiative losses in the four flames. Therefore experimental validation of the predicted flame temperature variation with ambient Le was sought. Three flames were studied in the 2.2 s drop tower with the thin-filament pyrometer and were modeled numerically. The flames include ethylene Flame (d) and corresponding flames burning methane and propane fuels, as summarized in Table 2. Fuel dilution levels were selected such that the adiabatic flame temperatures of the three flames was 2370 K. The ambient Le of the methane flame is less than that of ethylene flame while the ambient Le of the propane flame is higher. Flowrates in Table 2 were selected such that the ethylene and propane flame sizes were similar at 1.9 s, but limited access to the drop tower resulted in the methane flame radius being about 10% smaller. Nevertheless, these conditions are expected to yield comparable radiative loss fractions for these flames, and thus the effects of Le can be delineated.

The measured relative temperatures shown in Table 2 were determined by TFP. Compared to the ethylene flame, these results reveal that the methane and propane flames have increased and decreased peak temperatures, respectively, as is expected from their ambient Lewis numbers. Transient numerical predictions, also shown in Table 2, support these trends. The quantitative agreement between measured and modeled relative temperatures is adequate given uncertainties in the TFP measurements and possible residual ignition effects.

V. Conclusions

Novel aspects of spherical diffusion flames were examined. The work sought theoretical and computational insight into flame size, temperature, gaseous radiation, intermediate species loss, and Lewis number effects for four very different flame types: fuel (ethylene) into air, air into fuel, diluted fuel into oxygen and oxygen into diluted fuel. Where possible, the results were compared with microgravity measurements, emphasizing these four diffusion flames, which had different stoichiometric mixture fractions and convection directions.

The transient flame code predicted the temporal development of flame radius in 5 s tests, but accurate prediction of flame sizes were only obtained when transport properties were increased by 30% or when flow rates were decreased by 25%. Spherical flames with various convection directions and stoichiometric mixture fractions (at constant adiabatic flame temperature) reveal that in general there is a decrease in peak temperature with an increase in flame size. This is attributed to increased gas-phase radiative losses in large flames. Nonetheless, residence time also affects flame temperature. For the inverse spherical diffusion flame, where the fuel is in the ambient, intermediate species can be lost to the ambient, which can result in a small reduction in flame temperature. Finally, ambient Lewis number was found to have a profound effect on flame temperature for flames with long residence times provided that the flames are steady and nonradiating. For example, for Le near unity, a 10% decrease in Le is predicted to increase flame temperature by 200 K in these spherical diffusion flames. Nonetheless, the flame temperatures of the unsteady, radiating flames of this study were not strongly affected by Le.

Acknowledgments

References

[1]Atreya, A., and Agrawal, S., "Effect of Radiative Heat Loss on Diffusion Flames in Quiescent Microgravity Atmosphere," *Combust. Flame*, Vol. 115, 1998, pp. 372-383.

[2]Tse, S. D., Zhu, D., Sung, C.-J., Ju, Y., and Law, C. K., "Microgravity Burner-Generated Spherical Diffusion Flames: Experiment and Computation," *Combust. Flame*, Vol. 125, 2001, pp. 1265-1278.

[3]Christiansen, E. W., Tse, S. D., and Law, C.K., "A Computational Study of Oscillatory Extinction of Spherical Diffusion Flames." *Combust. Flame*, Vol. 134, 2003, pp. 327-337.

[4]Sunderland, P. B., Axelbaum, R. L., Urban, D. L., Chao, B. H., and Liu, S., "Effects of Structure and Hydrodynamics on the Sooting Behavior of Spherical Microgravity Diffusion Flames," *Combust. Flame* Vol. 132, 2003, pp. 25-33.

[5]Sunderland, P. B., Urban, D. L., Stocker, D. P., Chao, B. H., and Axelbaum, R. L., "Sooting Limits of Microgravity Spherical Diffusion Flames in Oxygen-Enriched Air and Diluted Fuel," *Combust. Sci. Tech.* Vol. 176, 2004, pp. 2143-2164.

[6]Law, C. K., and Chung, S. H., "Steady State Diffusion Flame Structure with Lewis Number Variations," *Combust. Sci. Tech.*, Vol. 29, 1982, pp. 129-145.

[7]Chung, S. H., and Law, C. K., "Structure and Extinction of Convective Diffusion Flames with General Lewis Numbers," *Combust. Flame*, Vol. 52, 1983, pp. 59-79.

[8]Mills, K., and Matalon, M., "Burner-Generated Spherical Diffusion Flames," *Combust. Sci. Tech.*, Vol. 129, 1997, pp. 295-319.

[9]Kee, R. J., Grcar, J. F., Smooke, M. D., Miller, J. A., and Meeks, E., "A Program for Modeling Steady, Laminar, One-Dimensional Premixed Flames," Sandia National Laboratories, Report No. SAND85-8240, 1987.

[10]Rothman, L. S., Rinsland, C. P., Goldman, A., Massie, S. T., Edwards, D. P., Flaud, J.-M., Perrin, A., Camy-Peyret, C., Dana, V., Mandin, J.-Y., Schroeder, J., Mccann, A., Gamache, R. R., Wattson, R. B., Yoshino, K., Chance, K. V., Jucks, K. W., Brown, L. R., Nemtchinov, V., and Varanasi, P., "The HITRAN Molecular Spectroscopic Database and Hawks (HITRAN Atmospheric Workstation): 1996 Edition," *J. Quantitative Spectroscopy and Radiative Transfer* Vol. 82, 2003, pp. 5-44.

[11]Carlson, B. G., and Lathrop, K. G., "Transport Theory - The Method of Discrete Ordinates," *Computing Methods in Reactor Physics,* edited by H. Greenspan, C. N. Kelber and D. Okrent, Gordon and Breach Science Publishers, New York, 1968.

[12]Grcar, J. F., "The Twopnt Program for Boundary Value Problems," Sandia National Laboratories, Report SAND91-8230, 1992.

[13]Kee, R. J., Rupley, F. M., and Miller, J. A., "Chemkin-II: A Fortran Chemical Kinetics Package for the Analysis of Gas Phase Chemical Kinetics," Sandia National Laboratories, Report SAND89-8009B, 1989.

[14]Kee, R. J., Dixon-Lewis, G., Warnatz, J., Coltrin, M. E., and Miller, J. A., "A Fortran Computer Code Package for the Evaluation of Gas Phase Multicomponent Transport Properties," Sandia National Laboratories, Report SAND86-8246, 1988.

[15]Smith, G. P., Golden, D. M., Frenklach, M., Moriarty, N. W., Eiteneer, B., Goldenberg, M., Bowman, C. T., Hanson, R. K., Song, S., Gardiner Jr., W. C., Lissianski, V. V., and Qin, Z., available at http://www.me.berkeley.edu/gri_mech/.

[16]Villimpoc, V., and Goss, L. P., "SiC-Based Thin-Filament Pyrometry: Theory and Thermal Properties," *Proc. Combust. Inst.*, Vol. 22, 1988, pp. 1907-1914.

[17]Pitts, W. M., "Thin-Filament Pyrometry in Flickering Laminar Diffusion Flames," *Proc. Combust. Inst.*, Vol. 26, 1996, pp. 1171-1179.

[18]Maun, J. D., Sunderland, P. B., and Urban, D.L., "Thin-Filament Pyrometry with a Digital Still Camera," *Applied Optics*, in press.

[19]Hirschfelder, J. O., Curtiss, C. F., and Bird, R. B., *Molecular Theory of Gases and Liquids*. Wiley and Sons, Hoboken NJ, 1964.

[20]Paul, P., and Warnatz, J., "A Re-evaluation of the Means Used to Calculate Transport Properties of Reacting Flows," *Proc. Combust. Inst.*, Vol. 27, 1998, pp. 495-504.

[21]Middha, P., Yang, B., and Wang, H, "A First-Principle Calculation of the Binary Diffusion Coefficients Pertinent to Kinetic Modeling of Hydrogen/Oxygen/Helium Flames," *Proc. Combust. Inst.*, Vol. 29, 2002, pp. 1361-1369.

[22]McBride, B. J., and Gordon, S., "Computer Program for Calculation of Complex Chemical Equilibrium Compositions and Applications," Report No. RP-1311-P2, NASA Lewis Research Center, 1996.